

VARIATIONAL MESSAGE PASSING-BASED RESPIRATORY MOTION ESTIMATION AND DETECTION USING RADAR SIGNALS

Jakob Möderl, Erik Leitinger, Franz Pernkopf, and Klaus Witrisal

Graz University of Technology, Graz, Austria (jakob.moederl@tugraz.at)

ABSTRACT

We present a variational message passing (VMP) approach to detect the presence of a person based on their respiratory chest motion using ultra-wideband (UWB) radar and to estimate the respiratory motion for contact-free vital sign monitoring. The received signal is modeled by a backscatter channel. The respiratory motion and propagation channel are estimated using VMP, while the presence of a person is detected by the evidence lower bound (ELBO). Numerical analyses and measurements demonstrate that the proposed method leads to a significant improvement in the detection performance compared to a fast Fourier transform (FFT)-based detector or an estimator-correlator, since the multipath components (MPCs) are better incorporated into the detection procedure. Specifically, the proposed method has a detection probability of 0.95 at -20 dB signal-to-noise ratio (SNR), while the estimator-correlator and FFT-based detector have 0.32 and 0.05, respectively.

Index Terms— Ultra-wideband radar, occupancy detection, variational message passing, vital sign estimation.

1. INTRODUCTION

Future cars will be required to detect if they are occupied when the car is being locked to prevent the confinement of small children, which makes detecting the presence of people a safety-critical application [1–3]. The respiratory motion of the chest provides a dynamic feature used to separate the target’s radar response from the strong clutter present in this use case [4]. We derive a Kronecker-factorized signal model for vital sign estimation in (strong) clutter using ultra-wideband (UWB) radar and present a variational message passing (VMP) algorithm [5, 6] to detect the presence of people and estimate the respiratory chest motion. An advantage of the derived model is, that it is linear in both the respiratory motion as well as the propagation channel and, thus, the message passing equations can be solved analytically.

Recent approaches to detect and estimate the respiratory chest motion based on radar responses are mostly based on

the intuition that the respiratory motion is periodic. They apply techniques such as fast Fourier transform (FFT) processing, principal component analysis or energy detection [7–11]. However, this assumption is easily violated, e.g. by infants who regularly experience apnea (short pauses with no respiration) [12]. This is especially important, considering that infants are very hard to detect in the first place, due to the small radar cross section and respiratory motion amplitude. Other works such as [13, 14] rely on a data-driven approach, which is typically limited by the small and heterogeneous data sets available. None of these works explicitly models the propagation of multipath components (MPCs). However, in a tightly enclosed space, such as the interior of a car, the MPCs that interact with the target carry additional information and can be used to increase the signal-to-noise ratio (SNR), which is of critical importance in the given use case. In this work, we apply VMP to improve upon the results of [4], which already incorporates MPCs into the detection.

Notation: Bold lowercase letters denote column vectors and uppercase letters denote matrices. We define \mathbf{I} to be the identity matrix and $\mathbf{1} = [1, 1, \dots, 1]^T$ to be a vector of ones with appropriate length. We use \odot and \otimes to denote the Hadamard (element wise) and Kronecker product of two vectors or matrices, respectively. The real operator and matrix trace operator are denoted as $\text{Re}\{\cdot\}$ and $\text{tr}(\cdot)$. We use $\mathcal{N}(\mathbf{a}|\mathbf{b}, \mathbf{C})$ and $\mathcal{CN}(\mathbf{a}|\mathbf{b}, \mathbf{C})$ to denote that the vector \mathbf{a} is distributed with a multivariate Gaussian or multivariate complex Gaussian distribution with mean \mathbf{b} and covariance matrix \mathbf{C} . Similarly $\text{Ga}(a|\alpha, \beta)$ is used to denote that the variable a is gamma-distributed with shape parameter α and rate parameter β . The notation $\langle f(x) \rangle_{q(x)} = \int f(x)q(x)dx$ denotes the expectation over the function $f(x)$ with respect to the distribution $q(x)$ and $\mathbb{H}(p)$ denotes the differential entropy of the distribution p . We write $p(\mathbf{x})$ or $p(\mathbf{x}|\mathbf{y})$ as shorthands for $p_{\mathbf{x}}(\mathbf{x})$ and $p_{\mathbf{x}|\mathbf{y}}(\mathbf{x}|\mathbf{y})$.

2. SIGNAL MODEL

We consider the case of a person sitting in a car, without intentional body movement. However, the chest of the person expands and contracts continuously due to the persons respiration. We propose to model the chest movement in direction of the antenna $b_t(t)$ as the realization of a zero-mean Gaussian

This research was partly funded by the Austrian Research Promotion Agency (FFG) within the project SEAMAL Front (project number: 880598).

random process. We aim to detect the presence of the person and estimate $b_t(t)$ using UWB radar signals.

Let \mathbf{s} be N samples, equally spaced with spacing $\Delta f = f_s/N$, of the complex baseband representation of the transmit pulse $s(f)$ centred at carrier frequency f_c . Several repetitions of the pulse are transmitted at times $t = mT_{\text{rep}}$, $m \in \{0, 1, \dots, M-1\}$ from the antenna. After propagating over a time-varying channel with frequency response $\mathbf{h}(t)$, each signal $\mathbf{r}_m = \mathbf{h}(mT_{\text{rep}}) \odot \mathbf{s} + \mathbf{w}_m$ received at repetition m is corrupted by noise \mathbf{w}_m . The noise samples \mathbf{w}_m are generated by a noise process $W_m(f)$, which is modeled as additive white Gaussian noise with double-sided power spectral density $N_0/2$, and is assumed to be independent across m and f . Thus, \mathbf{w}_m is a circular symmetric complex Gaussian random vector with covariance $\mathbf{C}_w = \lambda^{-1}\mathbf{I}$ and precision $\lambda = T_s/N_0$.

In order to remove the clutter, the mean $\bar{\mathbf{r}}$ over m is subtracted and the signals $\tilde{\mathbf{r}}_m = \mathbf{r}_m - \bar{\mathbf{r}}$ are stacked into a column vector $\tilde{\mathbf{r}} = [\tilde{\mathbf{r}}_0^T, \tilde{\mathbf{r}}_1^T, \dots, \tilde{\mathbf{r}}_{M-1}^T]^T$. As we derive in the following subsection, the time-varying part of the received signal

$$\tilde{\mathbf{r}} = \mathbf{b}_t \otimes \mathbf{h}_s + \mathbf{w} \quad (1)$$

is given as the product of the respiratory motion $\mathbf{b}_t = [b_t(0), b_t(T_{\text{rep}}), \dots, b_t((M-1)T_{\text{rep}})] \in \mathbb{R}^M$ and a channel vector $\mathbf{h}_s \in \mathbb{C}^N$ in additive white Gaussian noise $\mathbf{w} = [\mathbf{w}_0^T, \mathbf{w}_1^T, \dots, \mathbf{w}_{M-1}^T]^T$. The channel \mathbf{h}_s includes the transmit pulse shape and does not change over time. To extend this model to the multi-sensor case, we stack the received signals $\tilde{\mathbf{r}} = [\tilde{\mathbf{r}}_{s1}^T, \tilde{\mathbf{r}}_{s2}^T, \dots, \tilde{\mathbf{r}}_{sK}^T]^T$ and $\mathbf{h}_s = [\mathbf{h}_{s1}^T, \mathbf{h}_{s2}^T, \dots, \mathbf{h}_{sK}^T]^T$ where $\tilde{\mathbf{r}}_{s1}$ to $\tilde{\mathbf{r}}_{sK}$ are the received signals from K sensors with respective channels \mathbf{h}_{s1} to \mathbf{h}_{sK} .

Since we apply a frequency selective prior to \mathbf{b}_t the resulting covariance \mathbf{C}_{b_t} is not full rank. Thus, all computations are performed in the eigenspace $\mathbf{b} = \mathbf{U}^T \mathbf{b}_t$ corresponding to the eigendecomposition $\mathbf{C}_{b_t} = \mathbf{U} \mathbf{C}_b \mathbf{U}^T$, where \mathbf{C}_b is a diagonal matrix with the non-zero eigenvalues of \mathbf{C}_{b_t} on its main diagonal and \mathbf{U} is a matrix with the corresponding eigenvectors. Therefore, $\tilde{\mathbf{r}}$ can be expressed either as a linear function of the breathing signal $\mathbf{b}_t = \mathbf{U} \mathbf{b}$ given the block-diagonal matrix $\mathbf{H} = \mathbf{I} \otimes \mathbf{h}_s$ or as a linear function of \mathbf{h}_s given the block-diagonal matrix $\mathbf{B} = \mathbf{U} \mathbf{b} \otimes \mathbf{I}$:

$$\begin{aligned} \tilde{\mathbf{r}} &= \mathbf{B} \mathbf{h}_s + \mathbf{w} \\ &= \mathbf{H} \mathbf{U} \mathbf{b} + \mathbf{w}. \end{aligned} \quad (2)$$

The likelihood of receiving $\tilde{\mathbf{r}}$ given \mathbf{b} , \mathbf{h}_s and λ is $p(\tilde{\mathbf{r}} | \mathbf{b}, \mathbf{h}_s, \lambda) = \mathcal{CN}(\tilde{\mathbf{r}} | \mathbf{H} \mathbf{U} \mathbf{b}, \lambda^{-1} \mathbf{I}) = \mathcal{CN}(\tilde{\mathbf{r}} | \mathbf{B} \mathbf{h}_s, \lambda^{-1} \mathbf{I})$.

2.1. Propagation environment and target model

The propagation environment is modeled as a time-varying backscatter channel [15] with frequency response

$$\mathbf{h}(t) = \mathbf{h}_t(t) \odot \mathbf{h}_{\text{fb}} + \mathbf{h}_c. \quad (3)$$

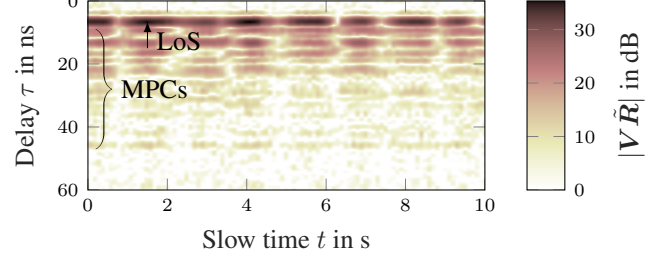


Fig. 1. Receive signal $\tilde{\mathbf{R}}$ of a radar measurement of an adult sitting on the back seat. The LoS component is visible at $\tau = 6$ ns and is modulated by the respiratory motion. Each row is approximately a scaled version of the row containing the LoS, as predicted by the derived signal model.

Introducing briefly the target channel $\mathbf{h}_t(t)$, the MPCs which interact with the target are modeled by a forward-backward channel $\mathbf{h}_{\text{fb}} = \mathbf{h}_f \odot \mathbf{h}_b$, which is the product of a forward channel \mathbf{h}_f covering the propagation from the transmit antenna to the target and a backward channel \mathbf{h}_b covering the propagation from the target back to the receive antenna. All other received MPCs are termed as clutter and are modeled by the frequency response \mathbf{h}_c . Since the target is assumed to be stationary, the channels \mathbf{h}_f , \mathbf{h}_b and \mathbf{h}_c can be assumed time-invariant as long as the respiratory motion $b_t(t)$ is much smaller than the smallest wavelength of the transmit signal.

The target is modeled as a single point target with a time-varying baseband frequency response $H_t(f, t) = \alpha e^{-j2\pi(f+f_c)\tau_b(t)}$, representing the reflection of the incoming signal by a coefficient $\alpha \in \mathbb{C}$ and a time-varying delay $\tau_b(t)$ induced by the respiratory motion $b_t(t)$. For a monostatic setup $\tau_b(t) = 2b_t(t)/c$, where c denotes the propagation speed of the signal. Using a first order Taylor-approximation $e^{-j2\pi(f+f_c)\tau_b(t)} \approx 1 - j2\pi(f+f_c)\tau_b(t)$, the sampled frequency response of the target changes over time as $\mathbf{h}_t(t) = \alpha(1 - j4\pi \frac{f+f_c}{c} b(t))$. Let $\mathbf{h}_s = -j4\pi\alpha/c \cdot \mathbf{h}_{\text{fb}} \odot (\mathbf{f} + f_c \mathbf{1}) \odot \mathbf{s}$, the received signal after clutter-removal at time m is $\tilde{\mathbf{r}}_m = b_t(mT_{\text{rep}}) \cdot \mathbf{h}_s + \mathbf{w}_m$. Thus, after stacking the signals $\tilde{\mathbf{r}}_m$ into a single vector, we arrive at (1).

Figure 1 shows a radar measurement of an adult sitting on the back seat of a car using a bandwidth of 500 MHz at a centre frequency of 6 GHz. The receive signal is stacked into a matrix $\tilde{\mathbf{R}} = [\tilde{\mathbf{r}}_1, \tilde{\mathbf{r}}_2, \dots, \tilde{\mathbf{r}}_{M-1}]$. To highlight the MPCs, the channel is transformed to time domain by the inverse-FFT matrix \mathbf{V} , where the $[k, n]$ -th element of \mathbf{V} is defined as $\frac{1}{\sqrt{N}} e^{j2\pi n k / N}$. The structure observed in the measurement is in accordance with the derived signal model and there is significant energy in the MPCs, which is used to increase the detection performance.

3. VARIATIONAL MESSAGE PASSING

Obtaining the maximum a-posteriori solutions for \mathbf{b} and \mathbf{h}_s is computationally infeasible due to the large dimen-

sions of \mathbf{b} and \mathbf{h}_s . Therefore, we apply a structured mean-field approach to approximate the posterior distribution $p(\mathbf{b}, \mathbf{h}_s, \lambda | \tilde{\mathbf{r}}) \propto p(\tilde{\mathbf{r}} | \mathbf{b}, \mathbf{h}_s, \lambda) p(\mathbf{b}) p(\mathbf{h}_s) p(\lambda)$ with a factorized distribution $q_1(\mathbf{b}, \mathbf{h}_s, \lambda) = q_b(\mathbf{b}) q_h(\mathbf{h}_s) q_\lambda(\lambda)$ [16]. VMP is applied to minimize the Kullback-Leibler divergence $\mathcal{D}_{\text{KL}}(q_1 \| p(\mathbf{b}, \mathbf{h}_s, \lambda | \tilde{\mathbf{r}}))$ of the true posterior $p(\mathbf{b}, \mathbf{h}_s, \lambda | \tilde{\mathbf{r}})$ from $q_1(\mathbf{b}, \mathbf{h}_s, \lambda)$ by maximizing the evidence lower bound (ELBO) [5, 17–20]. The ELBO is maximized using coordinate ascent, iteratively maximizing the ELBO with respect to one distribution $q_j \in \mathcal{Q} = \{q_b, q_h, q_\lambda\}$ by

$$q_j \propto \exp \left\{ \left\langle \ln p(\mathbf{b}, \mathbf{h}_s, \lambda | \tilde{\mathbf{r}}) \right\rangle_{q_j} \right\} \quad (4)$$

while keeping the remaining distributions $q_{\bar{j}} = \prod_{q_k \in \mathcal{Q} \setminus q_j} q_k$ fixed. Note, that the fixed point can be found analytically, if conjugate priors are used. Therefore, we assume a zero-mean Gaussian prior $p(\mathbf{b}) = \mathcal{N}(\mathbf{b} | \mathbf{0}, \mathbf{C}_{b_0})$ and a circularly-symmetric complex Gaussian prior $p(\mathbf{h}_s) = \mathcal{CN}(\mathbf{h}_s | \mathbf{0}, \mathbf{C}_{h_0})$ for the respiratory motion and channel vectors, respectively, and Jeffrey's prior $p(\lambda) \propto \lambda^{-1}$ for the noise precision λ . The resulting distributions $q_b(\mathbf{b}) = \mathcal{N}(\mathbf{b} | \hat{\mathbf{b}}, \hat{\mathbf{C}}_b)$, $q_h(\mathbf{h}_s) = \mathcal{CN}(\mathbf{h}_s | \hat{\mathbf{h}}_s, \hat{\mathbf{C}}_h)$, and $q_\lambda(\lambda) = \text{Ga}(\lambda | NM, \hat{M}_\lambda)$ are fully described by the parameters $\hat{\mathbf{b}}$, $\hat{\mathbf{C}}_b$, $\hat{\mathbf{h}}_s$, $\hat{\mathbf{C}}_h$ and $\hat{M}_\lambda = NM / \hat{\lambda}_1$. Let $\hat{E}_b^{[i]} = \text{tr}(\hat{\mathbf{C}}_b^{[i]}) + \|\hat{\mathbf{b}}^{[i]}\|^2$ and $\hat{E}_h^{[i]} = \text{tr}(\hat{\mathbf{C}}_h^{[i]}) + \|\hat{\mathbf{h}}_s^{[i]}\|^2$, the following messages are computed at iteration i :

$$\hat{\mathbf{C}}_h^{[i]} = (\mathbf{C}_{h_0}^{-1} + \hat{\lambda}_1^{[i-1]} \hat{E}_b^{[i-1]} \mathbf{I})^{-1} \quad (5)$$

$$\hat{\mathbf{h}}_s^{[i]} = \hat{\lambda}_1^{[i-1]} \hat{\mathbf{C}}_h^{[i]} \hat{\mathbf{B}}^{[i-1]} \mathbf{H} \tilde{\mathbf{r}} \quad (6)$$

$$\hat{\mathbf{C}}_b^{[i]} = (\mathbf{C}_{b_0}^{-1} + 2\hat{\lambda}_1^{[i-1]} \hat{E}_h^{[i-1]} \mathbf{I})^{-1} \quad (7)$$

$$\hat{\mathbf{b}}^{[i]} = 2\hat{\lambda}_1^{[i-1]} \hat{\mathbf{C}}_b^{[i]} \mathbf{U}^T \text{Re}\{\hat{\mathbf{H}}^{[i]} \mathbf{H} \tilde{\mathbf{r}}\} \quad (8)$$

$$\hat{\lambda}_1^{[i]} = \frac{NM}{\|\tilde{\mathbf{r}}\|^2 - 2\hat{\mathbf{b}}^{[i]T} \mathbf{U}^T \text{Re}\{\hat{\mathbf{H}}^{[i]} \mathbf{H} \tilde{\mathbf{r}}\} + \hat{E}_b^{[i]} \hat{E}_h^{[i]}}. \quad (9)$$

After initializing the messages as $\hat{\lambda}_1^{[0]} = NM / \|\tilde{\mathbf{r}}\|^2$, $\hat{\mathbf{C}}_b^{[0]} = \mathbf{C}_{b_0}$, and $\hat{\mathbf{b}}^{[0]}$ as a realization drawn from the prior $p(\mathbf{b})$, equations (5) through (9) are iterated until the messages are converged. Furthermore, $\hat{\mathbf{C}}_b^{[i]}$ is calculated by adding a scaled identity matrix to the inverse prior $\mathbf{C}_{b_0}^{-1}$. Therefore, the eigenvectors \mathbf{U} do not change throughout the iterations and can be precomputed based on the chosen prior \mathbf{C}_{b_0} .

To keep the notation concise, we refrain from explicitly writing iteration indices in the remainder of the paper, referring to the respective values after they are converged.

3.1. Detection

In order to detect the presence of a person, we need to distinguish between two nested models \mathcal{H}_0 and \mathcal{H}_1 , with corresponding likelihoods: $p(\tilde{\mathbf{r}} | \mathbf{b} = \mathbf{0}, \mathbf{h}_s = \mathbf{0}, \lambda, \mathcal{H}_0) = \mathcal{CN}(\tilde{\mathbf{r}} | \mathbf{0}, \lambda^{-1} \mathbf{I})$ of an empty car, and: $p(\tilde{\mathbf{r}} | \mathbf{b}, \mathbf{h}_s, \lambda, \mathcal{H}_1) = \mathcal{CN}(\tilde{\mathbf{r}} | \mathbf{B} \mathbf{h}_s, \lambda^{-1} \mathbf{I})$ if a person is present. Since the ELBO,

as the name suggests, is a lower bound on the logarithmic model evidence $\ln p(\mathcal{H}_i | \tilde{\mathbf{r}})$, we approximate the log odds ratio $\ln \mathcal{O} = \ln \frac{p(\mathcal{H}_1 | \tilde{\mathbf{r}})}{p(\mathcal{H}_0 | \tilde{\mathbf{r}})} \approx \mathcal{L}(q_1) - \mathcal{L}(q_0)$. The ELBO is calculated as $\mathcal{L}(q_k) = \left\langle \ln p(\mathbf{b}, \mathbf{h}_s, \lambda, \mathcal{H}_k | \tilde{\mathbf{r}}) \right\rangle_{q_k(\mathbf{b}, \mathbf{h}_s, \lambda)} + \mathbb{H}(q_k)$ for $k \in \{0, 1\}$ [5]. Since $q_0(\mathbf{b}, \mathbf{h}_s, \lambda) = q_0(\lambda)$ depends only on one parameter, we do not need an iterative update scheme and the ELBO $\mathcal{L}(q_0)$ is maximized by $q_0(\lambda) = \text{Ga}(\lambda | NM, \|\tilde{\mathbf{r}}\|^2)$, resulting in $\hat{\lambda}_0 = NM / \|\tilde{\mathbf{r}}\|^2$. Special considerations must be made regarding the improper prior $p(\lambda) \propto \lambda^{-1}$. Using a proper prior $p(\lambda) = \text{Ga}(\lambda | a, b)$ and taking the limit as $a, b \rightarrow 0$, the test decides for \mathcal{H}_1 if

$$\begin{aligned} & \frac{1}{2} \left[-\ln \det(\mathbf{C}_{b_0}) - \hat{\mathbf{b}}^T \mathbf{C}_{b_0}^{-1} \hat{\mathbf{b}} - \text{tr}(\mathbf{C}_{b_0}^{-1} \hat{\mathbf{C}}_b) \right] + \mathbb{H}(q_b) \\ & - \ln \det(\mathbf{C}_{h_0}) - \hat{\mathbf{h}}_s^H \mathbf{C}_{h_0}^{-1} \hat{\mathbf{h}}_s - \text{tr}(\mathbf{C}_{h_0}^{-1} \hat{\mathbf{C}}_h) + \mathbb{H}(q_h) \\ & + (NM - 1) \ln \frac{\hat{\lambda}_1}{\hat{\lambda}_0} + \mathbb{H}(q_\lambda) - \mathbb{H}(q_0) > \gamma \end{aligned} \quad (10)$$

is larger than the threshold γ .

4. RESULTS

To evaluate the performance of the devised algorithm, we consider the case of a single target sitting in a car while a monostatic radar transmits raised-cosine pulses with a bandwidth of 500 MHz and a roll-off factor of 0.5 at a centre frequency of $f_c = 6.5$ GHz, corresponding to the UWB channel 5 in [21]. A pulse is transmitted every $T_{\text{rep}} = 0.1$ s during a measurement duration of 10 s. The forward and backward channels \mathbf{h}_f and \mathbf{h}_b are simulated with an LoS component with power E_{LoS} at a delay of $\tau_0 = 1$ m/c. The LoS component is followed by a diffuse multipath with exponentially decaying power delay profile with decay constant τ_f . Thus \mathbf{h}_f and \mathbf{h}_b are described by the covariance $\mathbf{C}_{h_f}[n, n'] = \mathbf{C}_{h_b}[n, n'] = [E_{\text{LoS}} + \frac{E_{\text{DM}}}{\tau_f} (1 + j2\pi\tau_f \Delta f(n - n'))^{-1}] e^{-j2\pi\tau_0 \Delta f(n - n')}$. We choose $\tau_f = 20$ ns and E_{DM} such that $K_{\text{LoS}} = \frac{E_{\text{LoS}}}{E_{\text{DM}}} = 0.75$, since these values were observed by test measurements.

If the delay of the LoS component is known, the prior covariance \mathbf{C}_{h_0} can be calculated from $\mathbf{C}_{h_f}[n, n']$. However, we do not assume the distance to the target to be known a-priori. Thus, we calculate the covariance \mathbf{C}_{h_0} from a reparametrized covariance where $E_{\text{LoS}} = 0$ to remove the LoS component and $\tau_0 = 0.3$ m/c, corresponding to the minimum distance between the target and the radar sensor. This choice of prior enhances the detection performance compared to a flat prior by incorporating the decay constant of the channel without requiring the target distance to be known. The typical respiratory frequency for an adult is between 9 and 21 breaths per minute [22], where as the respiratory frequency of babies can go as high as 60 breaths per minute [12]. Therefore, we assume a prior covariance \mathbf{C}_{b_0} with a rectangular double sided power spectral density $S_b(f) = \frac{1}{2(f_{b,\text{max}} - f_{b,\text{min}})}$ for $f_{b,\text{min}} \leq |f| \leq f_{b,\text{max}}$ and 0 elsewhere, and select $f_{b,\text{min}} = 9/60$ Hz and $f_{b,\text{max}} = 1$ Hz.

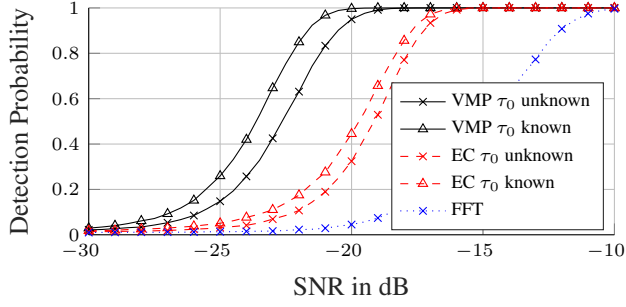


Fig. 2. Detection performance of the VMP-based detector compared to an estimator-correlator (EC) and FFT detector on simulated data.

To evaluate the performance, a Monte-Carlo simulation with 10^5 runs was performed at each $\text{SNR} = \frac{\lambda \|\mathbf{b}\|^2 \|\mathbf{h}_s\|^2}{NM}$ from -30 dB to 10 dB in 0.5 dB steps. The threshold for all detectors was set such that a constant false alarm rate of $p_{\text{FA}} = 0.01$ was achieved at each SNR value. As comparison, we evaluated the detection performance of an estimator-correlator, which models $\tilde{\mathbf{r}}$ as a Gaussian process to incorporate MPCs into the detection [4], and an FFT-based detector which computes the FFT over the rows of the matrix $\mathbf{V}\tilde{\mathbf{R}}$ and compares the peak against a threshold. For the FFT-based approach the channel is transformed to the time domain to concentrate the signal energy in the delay bin corresponding to the LoS component for easier detection. However, no MPCs are incorporated in the detection.

The results are depicted in Fig. 2. The proposed VMP-based algorithm has a better detection rate compared to the two other methods, even when using the modified prior which does not require a-priori knowledge of the distance to the target. Specifically, at an SNR of -20 dB, the VMP-based detection achieves a detection rate of approximately 0.95 while the estimator-correlator achieves 0.32 and the FFT detector achieves 0.05 in case the target distance is not known. This difference in performance can be explained by the different level of incorporation of the signal model into the detection: The VMP-based detector incorporates the signal model more rigidly in the detection compared to the estimator-correlator, which only accounts for the correlation between different columns of the matrix $\tilde{\mathbf{R}}$, or the FFT-based detector, which does not account for MPCs at all.

A measurement campaign including 34 participants (6 female and 28 male) was performed during which 177 minutes of data with a sample rate of $T_{\text{rep}} = 0.1$ s have been collected in total. The participants were instructed to sit motionless in the car while breathing normally. The measurements were performed using an M-sequence channel sounder in two different cars: a Seat Leon and a Citroen Picasso. The measurement equipment including channel sounder, cables and connectors has been calibrated before the measurement and the

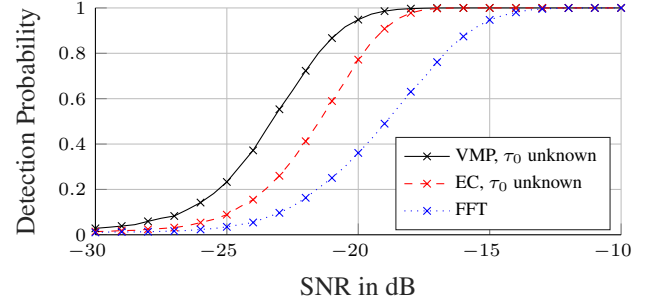


Fig. 3. Detection performance of the VMP-based detector compared to an estimator-correlator (EC) and FFT detector on measurement data with added noise.

same transmit pulse was used as in the simulations. The data was split in to non-overlapping chunks of 10 s length, for a total of 1046 measurements. For each SNR value, 100 independent noise realizations were added to the measurements to achieve the desired SNR for a total of 10^5 realizations. The resulting detection performance is shown in Fig. 3. The FFT-based approach performs significantly better on the measured data compared to the simulated data, since the respiratory motion of adults is closer to a periodic signal and has less randomness than the Gaussian process used in the simulations. Although the performance difference between the VMP-based approach and the other methods is less than in the simulations, the best detection probability is still achieved by the VMP-based detector.

5. CONCLUSION

We present a novel VMP-based approach to detect the presence of a person by their respiratory chest motion using UWB radar signals. The devised algorithm significantly outperforms the comparison methods on simulated as well as measured data. The superior performance of the presented detection algorithm is achieved through the use of MPCs, which are shown to carry a significant amount of signal energy in small spaces, such as the interior of a car. Additionally, the devised algorithm can be used for contact-free vital sign estimation since the respiratory chest motion is estimated as part of the algorithm. However, the received signal $\tilde{\mathbf{r}}$ depends on the product of \mathbf{b} and \mathbf{h}_s which results in an ambiguity in the sign of $\hat{\mathbf{b}}$ and $\hat{\mathbf{h}}_s$. Furthermore, deviations from a strictly periodic respiration pattern, such as pauses with different length in between breaths do not impact the performance of the devised algorithm, since the respiratory motion $b_t(t)$ is modeled as a random process and not as a periodic function.

Since many future cars will be equipped with UWB nodes, e.g. as part of the keyless entry system, the developed algorithm provides occupancy sensing capabilities to these cars without the need and increased manufacturing costs of dedicated sensors.

6. REFERENCES

- [1] Euro NCAP. (2021, May) Euro NCAP 2025 roadmap. [Online]. Available: <https://cdn.euroncap.com/media/30701/euroncap-roadmap-2025-v4-print.pdf>
- [2] Q. Xu, B. Wang, F. Zhang, D. S. Regani, F. Wang, and K. J. R. Liu, "Wireless AI in smart car: How smart a car can be?" *IEEE Access*, vol. 8, pp. 55 091–55 112, Mar. 2020.
- [3] A. S. Aghaei, B. Donmez, C. C. Liu, D. He, G. Liu, K. N. Plataniotis, H.-Y. W. Chen, and Z. Sojoudi, "Smart driver monitoring: When signal processing meets human factors: In the driver's seat," *IEEE Signal Process. Mag.*, vol. 33, no. 6, pp. 35–48, Nov. 2016.
- [4] J. Möderl, F. Pernkopf, and K. Witrisal, "Car occupancy detection using UWB radar," in *2021 18th Eur. Radar Conf.*, London, U.K., Apr. 5–7, 2022, pp. 313–316.
- [5] J. Winn, C. M. Bishop, and T. Jaakkola, "Variational message passing," *Journal of Machine Learning Research*, vol. 6, no. 4, p. 661–694, Apr. 2005.
- [6] C. M. Bishop, "Approximate inference," in *Pattern recognition and machine learning*, 8th ed., M. Jordan, J. Kleinberg, and B. Schölkopf, Eds. New York, NY, USA: Springer Science+Business Media, LLC, 2009, ch. 10, pp. 461–522.
- [7] Z. Baird, I. Gunasekara, M. Bolic, and S. Rajan, "Principal component analysis-based occupancy detection with ultra wideband radar," in *2017 IEEE 60th Int. Midwest Symp. on Circuits and Syst.*, Aug. 6–9, 2017, pp. 1573–1576.
- [8] A. Ahmad, J. C. Roh, D. Wang, and A. Dubey, "Vital signs monitoring of multiple people using a FMCW millimeter-wave sensor," in *2018 IEEE Radar Conf.*, Oklahoma City, OK, USA, Apr. 23–27, 2018, pp. 1450–1455.
- [9] L. Anitori, A. de Jong, and F. Nennie, "FMCW radar for life-sign detection," in *2009 IEEE Radar Conf.*, Pasadena, CA, USA, May 4–8, 2009, pp. 1–6.
- [10] Y. Kilic, H. Wymeersch, A. Meijerink, M. J. Bentum, and W. G. Scanlon, "Device-free person detection and ranging in UWB networks," *IEEE J. Sel. Topics Signal Process.*, vol. 8, no. 1, pp. 43–54, Feb. 2014.
- [11] D. Yang, Z. Zhu, J. Zhang, and B. Liang, "The overview of human localization and vital sign signal measurement using handheld IR-UWB through-wall radar," *Sensors*, vol. 21, no. 2, May 2021.
- [12] U. Frey, M. Silverman, A. L. Barabási, and B. Suki, "Irregularities and power law distributions in the breathing pattern in preterm and term infants," *J. Appl. Physiol.*, vol. 85, no. 3, pp. 789–797, Sep. 1998.
- [13] Y. Ma, Y. Zeng, and V. Jain, "CarOSense: Car occupancy sensing with the ultra-wideband keyless infrastructure," *Proc. ACM Interact. Mobile Wearable Ubiquitous Technol.*, vol. 4, no. 3, Sep. 2020.
- [14] M. Alizadeh, H. Abedi, and G. Shaker, "Low-cost low-power in-vehicle occupant detection with mm-wave FMCW radar," in *IEEE SENSORS*, Montreal, QC, Canada, Oct. 27–30, 2019, pp. 1–4.
- [15] D. Arnitz, U. Muehlmann, and K. Witrisal, "Wide-band characterization of backscatter channels: Derivations and theoretical background," *IEEE Trans. Antennas Propag.*, vol. 60, no. 1, pp. 257–266, Jan. 2012.
- [16] G. E. Kirkelund, C. N. Manchon, L. P. B. Christensen, E. Riegler, and B. H. Fleury, "Variational message-passing for joint channel estimation and decoding in MIMO-OFDM," in *2010 IEEE Global Telecommun. Conf.*, London, U.K., Dec. 6–10, 2010, pp. 1–6.
- [17] E. Riegler, G. E. Kirkelund, C. N. Manchon, M. A. Badiu, and B. H. Fleury, "Merging belief propagation and the mean field approximation: A free energy approach," *IEEE Trans. Inf. Theory*, vol. 59, no. 1, pp. 588–602, Jan. 2013.
- [18] C. Zhang, J. Bütepage, H. Kjellström, and S. Mandt, "Advances in variational inference," *IEEE Trans. Pattern Anal. Mach. Intell.*, vol. 41, no. 8, pp. 2008–2026, Aug. 2019.
- [19] T. Minka, "Divergence measures and message passing," Microsoft Res., Tech. Rep., 2005, accessed: Sep. 2022. [Online]. Available: <https://citeseerx.ist.psu.edu/viewdoc/download?doi=10.1.1.361.9105&rep=rep1&type=pdf>
- [20] D. M. Blei, A. Kucukelbir, and J. D. McAuliffe, "Variational inference: A review for statisticians," *J. Amer. Statistical Assoc.*, vol. 112, no. 518, pp. 859–877, Jul. 2017.
- [21] *IEEE Standard for Low-Rate Wireless Networks*, IEEE Std. 802.15.4-2020, Jul. 2020, (Revision of IEEE Std 802.15.4-2015).
- [22] S. H. Fairclough and L. J. M. Mulder, "Psychophysiological processes of mental effort investment," in *How motivation affects cardiovascular response: Mechanisms and applications*, R. A. Wright and G. H. E. Gendolla, Eds. Amer. Psychological Assoc., 2012, pp. 61–76.